Microsc. Microanal. Page 1 of 15
doi:10.1017/S1431927610093979

Microscopy AND Microanalysis

A New Look at Lunar Soil Collected from the Sea of Tranquility during the Apollo 11 Mission

Carol Kiely,[1,*] Gary Greenberg,[2] and Christopher J. Kiely[1]

[1]*Department of Materials Science and Engineering, Lehigh University, Bethlehem, PA 18015-3195, USA*
[2]*University of Hawaii, Institute of Astronomy, Advanced Technology Research Center, HI 96768, USA*

Abstract: Complementary state-of-the-art optical, scanning electron, and X-ray microscopy techniques have been used to study the morphology of Apollo 11 lunar soil particles (10084-47). The combination of innovative lighting geometries with image processing of a through focal series of images has allowed us to obtain a unique collection of high-resolution light micrographs of these fascinating particles. Scanning electron microscopy (SEM) stereo-pair imaging has been exploited to illustrate some of the unique morphological properties of lunar regolith. In addition, for the first time, X-ray micrographs with submicron resolution have been taken of individual particles using X-ray ultramicroscopy (XuM). This SEM-based technique lends itself readily to the imaging of pores, cracks, and inclusions and allows the internal structure of an entire particle to be viewed. Rotational SEM and XuM movies have also been constructed from a series of images collected at sequential angles through 360°. These offer a new and insightful view of these complex particles providing size, shape, and spatial information on many of their internal features.

Key words: optical microscopy, scanning electron microscopy, stereo microscopy, X-ray ultramicroscopy, lunar regolith

Introduction

On a clear night when the moon is full, it is quite easy to identify the region where the "Eagle" landed on July 20th, 1969. The Sea of Tranquility is one of a number of darker features—*the lunar maria*—visible on the lunar surface. Its color is due to a type of volcanic rock, basalt, which was formed by the cooling of lava flows that filled the lowlands over 3.8 billion years ago. Since then, the lunar surface has been subjected to continuous bombardment by micrometeors and constant exposure to the solar wind. The repeated fracture of the underlying bedrock caused by micrometeor bombardment has resulted in the lunar surface being covered by a fine charcoal gray powder.

During the Apollo 11 mission, astronauts Neil Armstrong, Buzz Aldrin, and Michael Collins brought back over 21 kg of rock and soil samples—*lunar regolith*. These precious samples have been extensively studied by geologists for over 40 years. For excellent review articles on the subject, see McKay et al. (1991), Lucey et al. (2006), and Lindsey (1976). The average particle size in the lunar soil is close to 70 μm, but some can be as large as 800 μm while many are less than 20 μm. Geologists also have a good idea of its mineral and chemical composition. Surprisingly, only 24% of the lunar soil is made up of basaltic rock fragments (Morris et al., 1983). The majority of the particles, approximately 52%, are *agglutinates*—agglomerates of mineral and glass fragments encased in a glassy matrix. These have formed during the impact of micrometeorites with the lunar surface. While the vast majority of micrometeorites have masses $<10^{-6}$ g, they are traveling at velocities close to 20 km s^{-1} (Lindsay & Srnka, 1975). The immense heat associated with such an impact causes the lunar soil to melt, and some of this molten regolith flows down between the underlying rock and mineral fragments. As it cools, it encases these underlying fragments in a vesicular glassy matrix. This type of particle has not been found anywhere on Earth. There are, of course, many other types of particles present in lunar soil such as tiny glass spheres, vesicular glass particles, glass shards, breccias, and several types of mineral fragments (e.g., calcium-rich plagioclase, olivine, pyroxene, and ilmenite). Most of these have formed as a result of micrometeor bombardment. There are some mainly solid glass spheres that are thought to have originated from the cooling of molten lava from fire fountain volcanoes that occurred early in the Moon's history (Heiken et al., 1974).

While numerous monochrome light micrographs of lunar soil particles can be found throughout the literature (e.g., Burlingame et al., 1970; Mueller & Hinsch, 1970; Bastin, 1980), few high magnification color micrographs have been published. The quality of the image obtained with an optical microscope is typically limited by the depth of field of the objective lens. This means that when trying to take a photograph of a particle, only a small part of it is in sharp focus at any one time; the foreground and background are often blurred. The greater the magnification, the worse this problem becomes. This limitation can now be overcome by collecting a systematic series of images while moving the focal plane stepwise from the top to the bottom of the particle. A computer software algorithm then analyzes each image and selects only the in-focus regions, discarding the out-of-focus parts. The in-focus portions are

Received March 11, 2010; accepted August 12, 2010
*Corresponding author. E-mail: cak4@lehigh.edu

then seamlessly joined into a single image that is totally in focus. This feature is available on some of today's more specialized computer controlled light microscopes (e.g., Pawley, 1995).

In addition, as any photographer will tell you, the way in which you light a subject is crucial to obtaining a good photograph. The same is true for taking a light micrograph through a microscope. Conventional microscopes have two basic illumination geometries: one that passes light through the sample (transmission) and the other where a beam of light is reflecting off it. This is not the best way to bring out the detail in a picture—the lighting is too "flat." It has been revealed (Greenberg & Boyde, 1993, 1997) that oblique lighting creates the strange effect of making the sample appear tilted in the microscope, as if you were looking at it from an angle: the more oblique the illumination angle, the greater the apparent degree of tilt. Oblique lighting from two different sources (one from the left and one from the right) can be directed through the sample to produce a left eye and right eye view simultaneously, resulting in a dramatic three-dimensional (3D) image. In other words, both eyes receive a two-dimensional (2D) image but from a slightly different angle; the human brain then naturally creates the third dimension. This approach has been used in a wide variety of applications, ranging from cancer screening (Ramsamooj et al., 2002) to a comparison of the morphology of sand grains from around the world (Greenberg, 2008). Using oblique lighting in conjunction with the collection and subsequent processing of a through-focal series of frames has allowed us to obtain high-resolution color micrographs of lunar regolith particles showing detail never thought possible with an optical microscope.

Numerous studies of individual lunar regolith particles have involved the use of scanning electron microscopy (SEM) for imaging and X-ray energy dispersive spectroscopy (XEDS) for chemical analysis (e.g., Carter & MacGregor, 1970*a*, 1970*b*; Chao et al., 1970; McKay et al., 1970; Nagy et al., 1970; Rode et al., 1979; Robens et al., 2007; Lui et al., 2008). These techniques, however, only yield information from the near surface regions of a particle. Much of the internal compositional information on lunar soil particles has been gleaned from petrographic analysis (e.g., Duke et al., 1970; Taylor et al., 1996), which usually requires the particles to be encased in epoxy resin, followed by slicing and polishing so that thin flat samples can be subsequently examined under a light or scanning electron microscope. This technique has several advantages, for example, slices of several particles can be viewed at the same time within a single petrographic sample making it relatively easy to distinguish between different rock types; however, information is only being gleaned from a single 2D slice of each particle. Until recently, this was only the viable method of examining the internal structure of such particles.

Now, there is a new technique called X-ray ultramicroscopy (XuM) that enables the internal structure of a whole particle to be imaged without having to slice or polish. Pioneered at the CSIRO, Australia (Wilkins et al., 1996), it utilizes the small spot source of X-rays generated in a scanning electron microscope when the electron beam is focused onto a metal target (usually platinum). The divergent X-ray beam then passes through the sample and a projection image is collected by an X-ray sensitive charge-coupled device camera (see the schematic diagram shown in Fig. 1). X-ray imaging of lunar regolith has only been carried out once before using the synchrotron beamline 13M (GSECARS) of the DOE Advanced Photon Source (Ebel et al., 2005); XuM, however, offers a much improved resolution. An excellent overview of the XuM technique has been given by Brownlow et al. (2006).

Table 1. Approximate Attenutation Lengths of Platinum X-Rays ($L_{\alpha 1}$-line: 9.442 keV) in a Variety of Substances.*

Material	Attenuation Length
$CaAl_2Si_2O_8$ (plagioclase)	180 μm
$(Ca,Mg,Fe,Al,Ti)_2Si_2O_6$ (pyroxene)	60–150 μm[a]
$(Mg,Fe)SiO_4$ (olivine)	68 μm[a]
TiO_2	26.5 μm
$FeTiO_3$ (ilmenite)	9.2 μm
FeO	7.4 μm
Fe	5.8 μm

*Data (approximate values) were taken from the Lawrence Berkeley Laboratory website: http://henke.lbl.gov/optical_constants/.
[a]Highly dependent on the amount of Fe present.

Unlike light microscopy, the entire XuM image is in focus. The magnification can be altered by simply moving the sample closer to or further away from the X-ray source. Contrast in a 2D X-ray projection image of a particle is governed by its chemical composition, thickness, and the energy of the incident X-rays. The absorbing power of a material is usually defined by an attenuation length, i.e., the thickness of material that causes the transmitted X-ray beam to lose $1/e$ of its initial intensity. Table 1 lists the attenuation lengths of platinum X-rays (Pt L_α line: 9.442 keV) for the most common minerals found in lunar soil. The attenuation lengths of the most abundant minerals lie between 60–180 μm, which means that X-ray ultramicroscopy is *ideally suited* to the study of the size range of particles found in lunar soil. Ilmenite ($FeTiO_3$) and metallic iron are considerably more absorbent than the more common minerals (e.g., $CaAl_2Si_2O_8$) contained in the regolith and, if present, are usually the darkest regions in the X-ray image.

Absorption is not the only contrast mechanism exhibited in an XuM image. Because the sample is so close to the source (typically less than 5 mm) and the detector is relatively far away (approximately 235 mm) and the X-ray beam is diverging, interference occurs between the incident waves and any diffracted waves generated from the edges of pores and boundaries within the sample. The result is a series of bright and dark fringes, which enhance the visibility of pores and cracks in the image.

One particularly useful feature of the XuM technique is the ability to collect images while rotating the sample step-

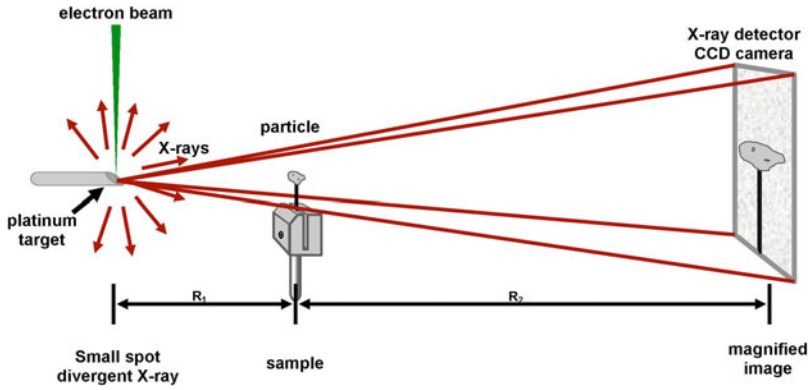

Figure 1. A schematic diagram of the X-ray ultramicroscope.

wise through 360°. Simply comparing two images, the second being collected with the particle oriented at 90° to the first, can help prevent erroneous conclusions being drawn from a single 2D projection image. For example, a plate-like inclusion could be mistakenly thought to be a needle-like inclusion when viewed "edge on" a single 2D projection image. A more informative 3D view of the internal structure of a particle can also be achieved by the construction of a rotational movie from a sequential series of images collected at different angles.

In this article, we exploit both new and well-established techniques in light, electron, and X-ray microscopy in an attempt to dispel the myth that lunar soil is just a fine gray powder.

Materials and Methods

All the lunar regolith particles imaged in this study were taken from a sample of Apollo 11 regolith (10084-47), which was on loan from the Johnson Space Research Center. Some particles were examined in the "as-received" state. A small portion of the regolith was placed into a test tube, suspended in ethanol, and agitated for a few minutes. The liquid fraction, containing a dispersion of smaller particles, was then pipetted into a second test tube. Both test tubes were then placed in an oven for 10 min at 110° to evaporate the alcohol. Most of the images shown in this article were of particles that had been washed in ethanol because this process removed most of the smaller submicron debris from their surfaces, facilitating a much clearer view of their internal structure.

For light microscopy analysis, a small sample of the washed regolith was placed on a cleaned glass slide. The particles were manipulated into position using a pristine acupuncture needle. The instrument used was an Edge-3D light microscope that utilizes a single objective lens (i.e., a conventional plan-apo lens) to capture high-definition images from left and right eye points of view simultaneously. Two modes of illumination were employed: (1) highly oblique reflected light was produced using fiber optic light guides positioned approximately 5 cm from the specimen at an angle of 10° above the horizon, and (2) oblique transmitted light was linearly polarized, and after passing through the specimen, an analyzer (a linear polarizer set at 90° to the illumination polarization) made the internal structure of the particles visible. In cases where high-magnification objective lenses were required, reflected light was directed onto the edge of the glass cover-slip, and total internal reflection though the cover-slip lit the underlying lunar particles. To produce a fully-focused 3D image, stacks of left- and right-eye images were acquired digitally at sequential focus steps starting with the top of the sample being in focus and progressing to the bottom. Helicon Focus software (Helicon Soft Ltd., Karkov, Ukraine) was used to analyze each image in the series, selecting the in-focus portions, and discarding the out-of-focus portions. All the in-focus portions were then seamlessly combined into a single image in which everything is in sharp focus.

For SEM and XuM analysis, individual particles were separated out under a stereo microscope using a pristine acupuncture needle. They were then glued onto a small carbon fiber/epoxy post that was supported in a specially designed sample holder (Fig. 1) and subjected to a very thin (<5 nm) coating of gold to minimize charging by stray secondary electrons inside the SEM. All the secondary electron imaging was carried out using an FEI XL30 ESEM (FEI Company, Hillsboro, OR, USA) operating in high-vacuum mode. A small stepper motor driven rotational stage was constructed that allowed the sample to be positioned at different angles with respect to the scanning electron detector. Rotational SEM movies were then made using Macromedia Fireworks software. The X-ray microscopy was also performed in the FEI XL30 ESEM using an XuM system designed by Gatan, Inc. (Pleasanton, CA, USA). To generate a small spot of X-rays, the electron beam (25 kV) was focused at a working distance of 6 mm onto a polished piece of platinum foil. The condenser lens setting and objective aperture size were chosen to optimize the X-ray flux for the desired XuM image resolution. Rotational XuM movies were made using Gatan's Digital Micrograph and Macromedia Fireworks software.

Permission was not given to perform any destructive techniques on these precious and historically important samples, so we were unable to perform any transmission electron microscopy analysis of individual particles to determine the crystal structure and identify the components of

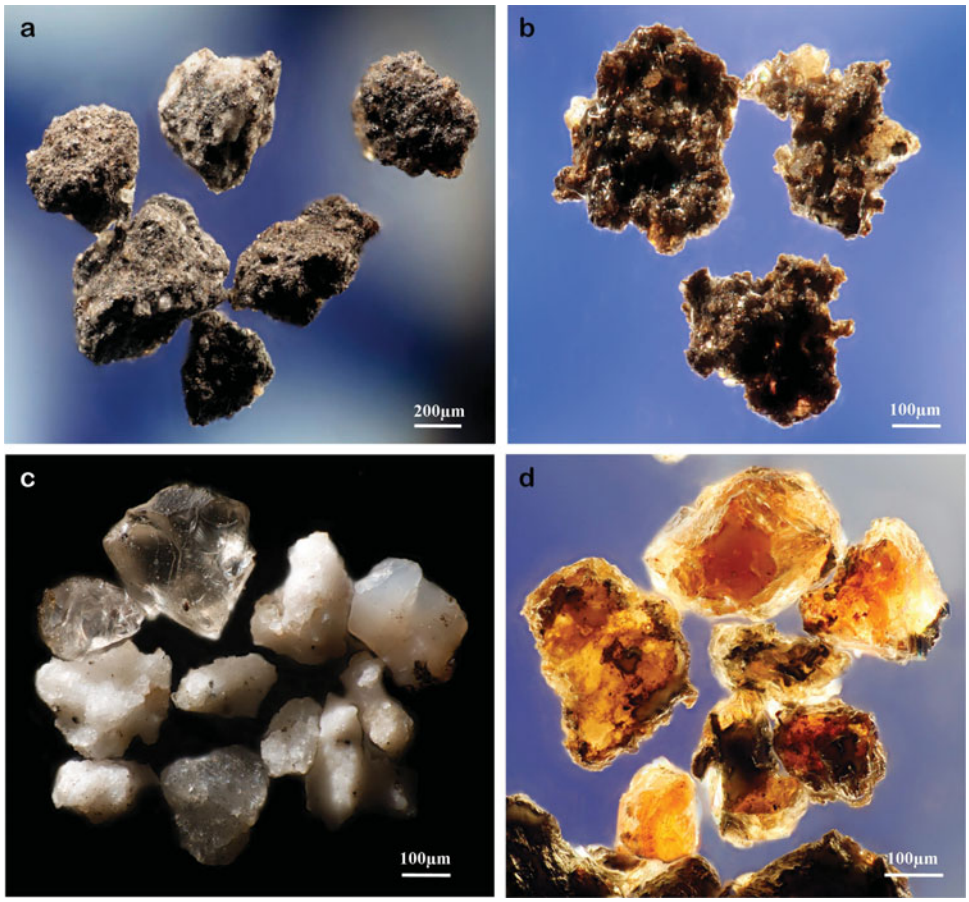

Figure 2. Optical micrographs of groups of different types of lunar regolith particles (**a**) basalt particles, (**b**) agglutinates, (**c**) a collection of glass and white anorthositic fragments, and (**d**) pyroxene based fragments showing signs of surface melting.

each individual particle. However, XEDS was used in an attempt to identify the composition of the individual particles.

Results and Discussion

Light Microscopy

Examples of light micrographs obtained by combining oblique lighting with the collection and subsequent processing of a through-focal series of frames are shown in Figures 2 and 3. Figure 2a is a relatively low magnification image of a group of basaltic fragments. These gray particles exhibit the characteristic fine-grained texture of basalt. The particle in the top right-hand corner, however, appears to have a slightly glossier surface suggesting that it has an outer glass coating characteristic of an agglutinate particle. Agglutinates come in many different shapes and sizes but their surfaces generally tend to exhibit a rounded form imposed by the viscosity and surface tension of the fluid glass. The three agglutinates (300–400 μm in size) shown in Figure 2b are typical of the mid-size range of agglutinate particles found in this regolith sample. The oblique lighting conditions clearly highlight the glassy nature of the matrix component of these particles and the myriad of different colored mineral, rock, and glass fragments contained within. There are, however, many other types of particles that fall within this size range. Figure 2c shows a group of particles ranging from clear glass to fine-grained white anorthosite fragments. The orange pyroxene particles shown in Figure 2d exhibit clear signs of surface melting together with inclusions of a much darker material.

One of the most interesting types of regolith particles are the glassy spherules. They come in a variety of colors: off-white, orange, red, brown, and dark gray. The darker particles contain more iron and titanium—a basaltic composition, whereas the lighter particles tend to contain more calcium and aluminum—closer to an anorthositic composition. The orange glassy spheroid shown in Figure 3a is thought to have originated from ancient fire fountain volcano (McKay et al., 1991). The tiny bubbles present in the near surface region are due to the release of volatile material at high temperatures when the sphere was molten. The vast majority of glass globules found in Apollo 11 lunar soil, however, are thought to be ejecta from primary micrometeor impacts. The energy associated with such impacts causes the regolith to melt and solidification occurs before the droplet returns to the lunar surface (Fox et al., 1970; Tolansky, 1970). Many of these spheres are opaque and possess bud-like protuberances (e.g., Fox et al., 1970; McKay et al., 1970), an example of which is shown in Figure 3b. Such spheroids have a much higher Fe and Ti content and are less homogeneous than the orange spheres. While many of these glassy particles are perfect spheres, other shapes such as ellipsoids, tear drops, rods, and dumbbells can also

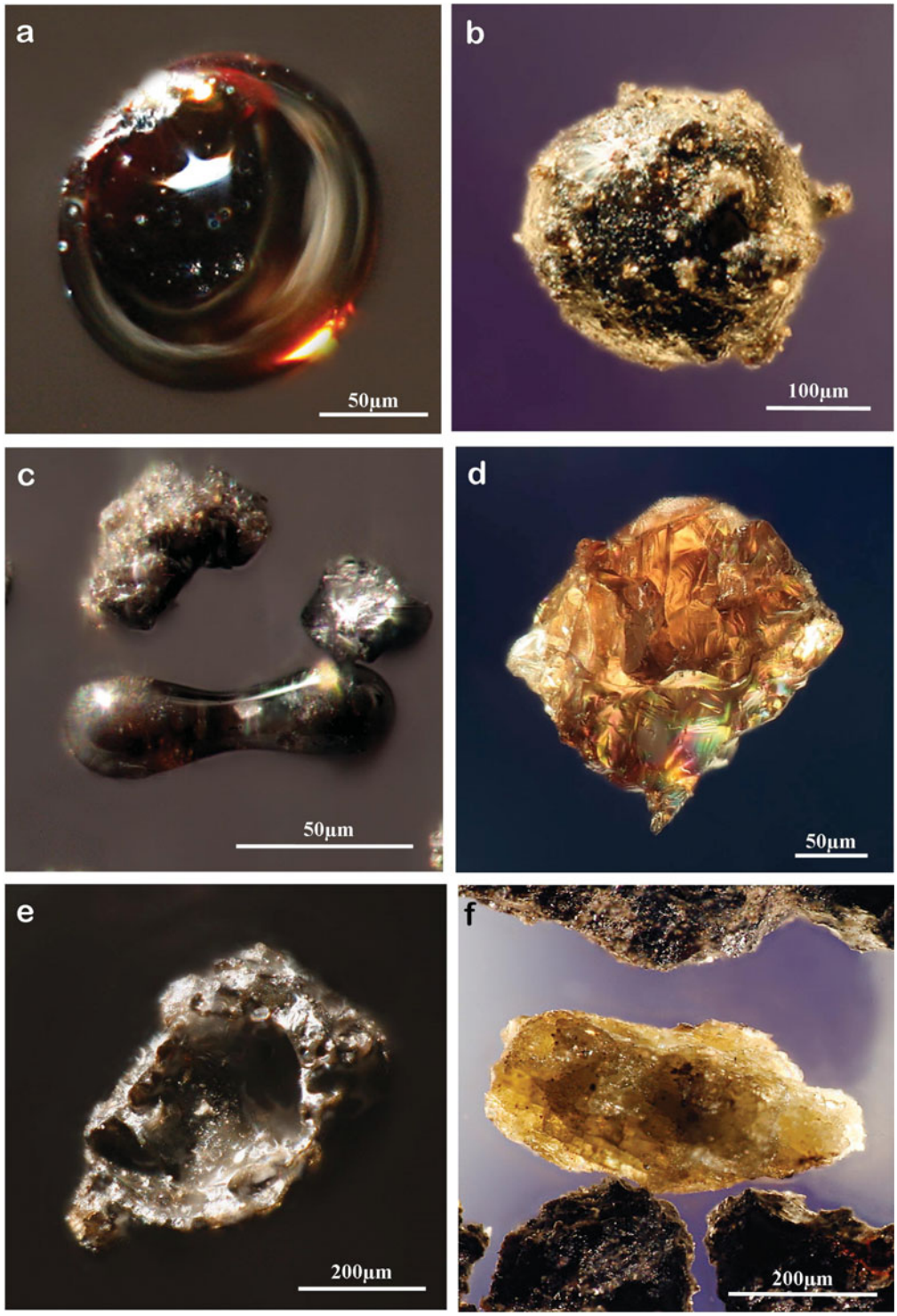

Figure 3. Optical micrographs of individual lunar regolith particles (**a**) orange glass sphere, (**b**) an opaque spherule with bud-like protuberances, (**c**) a glassy dumbbell, (**d**) a concave vesicular glass particle, (**e**) a gem-like particle, and (**f**) a white anorthosite particle showing signs of surface melting.

be found in lunar soil (e.g., Cloud et al., 1970; Fulchignoni et al., 1971; Mueller, 1971). An example of a glassy dumbbell particle is shown in Figure 3c.

The beautiful gem-like particle shown in Figure 3d may have started out as a pyroxene crystal, but along the way its original structure has been modified. The dark vertical lines appear to be mechanically induced where one section of the crystal has been sheared with respect to another, and there is also a region of birefringent material present. The 600 μm concave glassy particle shown in Figure 3e probably started its existence as an expanding bubble in a very viscous piece of molten regolith. The pressure inside the bubble eventu-

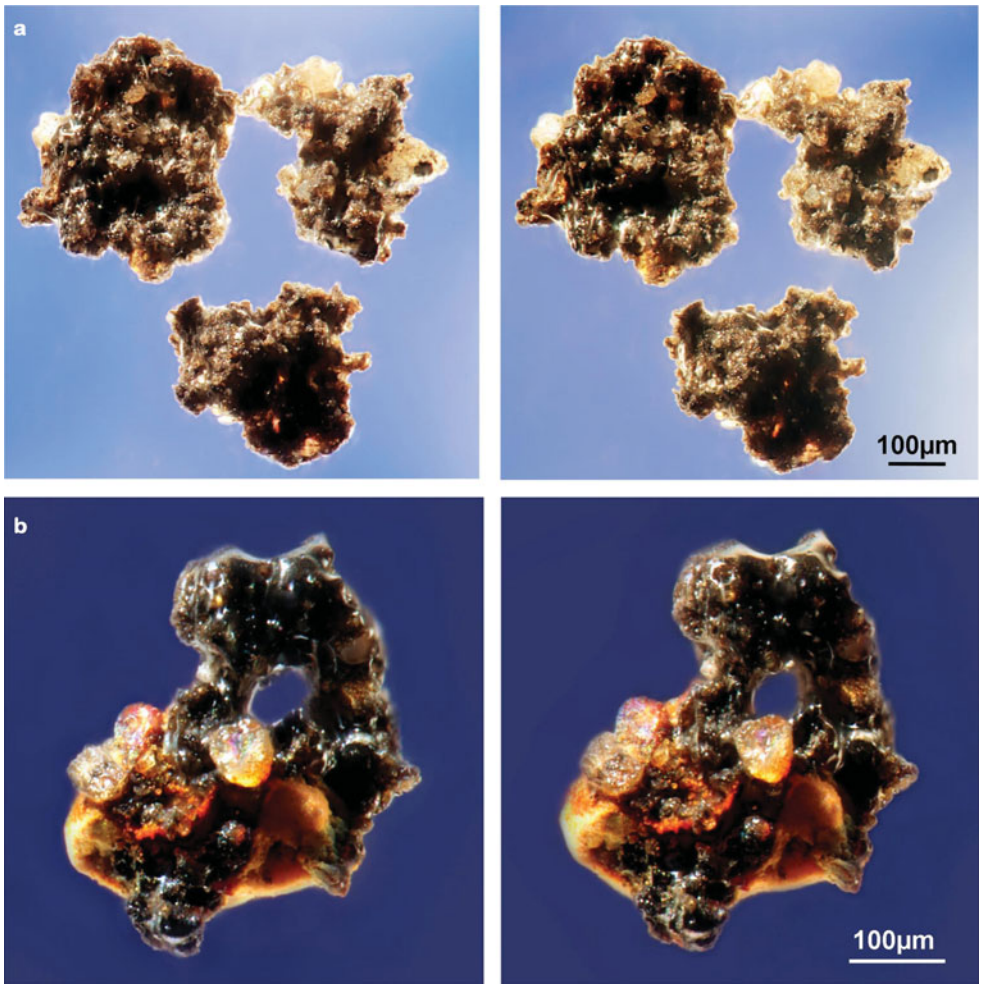

Figure 4. Optical stereo-pair micrographs of (**a**) three agglutinate particles, and (**b**) a "ring agglutinate" with mineral fragments adhering to its surface.

ally became too great, causing fracture rather than any further increase in the bubble diameter. The fragment shown, in Figure 3e, must have been exposed to intense heat causing its surface to flow and smooth out before solidifying. There is also clear evidence of surface melting in the micrograph of the off-white anorthosite particle shown in Figure 3f. This type of particle is thought to have originated from the highlands and been subsequently transported down onto the maria during successive meteor impacts.

Although these light micrographs illustrate the fascinating diversity of lunar regolith particles, they can sometimes give rise to misleading conclusions because they are 2D images. Take a look at the stereo-pair images presented in Figure 4a (slightly cross your eyes and focus on the central image to obtain the 3D effect). A 3D view makes it easier to see the variety of different components within the agglutinates. Rather than being completely enclosed in a glass matrix, the tiny rock and mineral fragments appear to be glued together in a random fashion to form a highly complex 3D structure. A more striking stereo-pair of a "ring" agglutinate is shown in Figure 4b. While many of its components have been encased completely in a dark glassy matrix, there are some larger mineral fragments that appear to be simply adhered to the outer surface. XEDS reveals that the orange region at the bottom of the particle in Figure 4b contains a very high proportion of iron whereas the main body of this agglutinate contains a complex mixture of calcium, aluminum, titanium, silicon, and iron oxides.

Scanning Electron Microscopy

SEM has proven to be a very powerful tool for studying the surface structure of lunar regolith particles and in particular those features that are beyond the resolution of a light microscope (e.g., Rode et al., 1979; McKay et al., 1991). Lunar regolith particles are also an ideal subject for the collection of stereo-pairs, an SEM technique that is often overlooked. In one of the first detailed SEM studies of Apollo 11 regolith (Carter & MacGregor, 1970*b*), it was mentioned that some of the features could not be seen clearly unless viewed stereoscopically. Since then, however, few, if any, researchers have taken advantage of this highly informative type of imaging. The stereo-pairs collected in this current study yield a much more intuitive understanding of the morphology of regolith particles.

When a micrometeorite strikes the lunar surface, the intense heat that is generated causes some of the underlying rock or regolith to melt, and as it cools, the molten mixture forms a glass. During this process, the more volatile components are released, resulting in gaseous bubbles forming within the melt. Some of these bubbles reach the surface

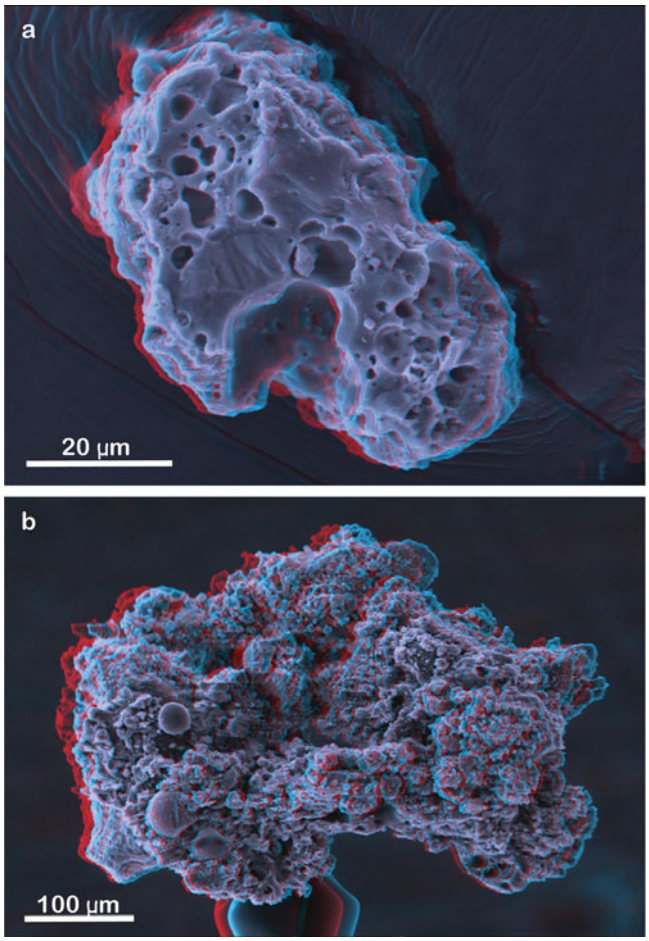

Figure 5. SEM stereo-anaglyphs of (**a**) a vesiculated glass particle and (**b**) a ring agglutinate.

while others remain trapped as the molten regolith solidifies. The identity of the gases responsible for bubble formation is not known for certain, but many researchers believe that they are a mixture of gases implanted by the solar wind (e.g., Pillinger, 1979). An anaglyph stereo SEM image of a vesiculated glass particle is shown in Figure 5a. Red/cyan glasses are needed to view these anaglyphs (*remember:* red on the left). This stereo-view gives a more accurate impression of the porosity of this type of particle and how the pores interconnect. XEDS analysis carried out on this particle reveals that it is comprised primarily of calcium aluminosilicate glass, but if you look more closely, there are a number of "dark stripes" that are plates of ilmenite encased in the glass.

As described previously, agglutinate particles comprise of a number of rock, mineral, and glass fragments encased in impact-melt glass. Often agglutinates have "ring" or "doughnut" structure, an example of which is shown in Figure 5b. Lindsay and Srnka (1975) explained that when a micrometeor strikes the lunar surface enough heat is generated to fuse together and even melt the underlying soil particles. Some of the melt is lost as spray during the initial crater formation. The rest of the impact melt flows into the spaces between the surrounding soil particles encasing them in a glassy matrix as it cools. They concluded that only one ring agglutinate can be formed from a single micrometeor strike. They also estimated that the mass of an agglutinate is approximately five times that of the impacting meteorite. Stereo-viewing naturally encourages one to examine the particles more closely and for a longer period of time. Notice the myriad of tiny fragments stuck to the surface. The pores in the glassy matrix at the bottom right-hand region of the particle in Figure 5b are open to the surface. The globules that appear on the left-hand side almost certainly have formed by the bubbling of molten glass, but in this case the bubbles have not broken through to the surface. An alternative method of obtaining a depth perspective view of the particle is to construct a rotational movie from a sequential series of micrographs collected with the particle at different angles with respect to the detector. A rotational movie of this ring agglutinate particle can be found in the supplementary on-line information that accompanies this article (see Supplementary Movie 1).

Supplementary Movie 1

Supplementary Movie 1 is an SEM rotational movie of a ring aggutinate. Please visit journals.cambridge.org/jid_MAM.

Figure 6 is a collection of higher magnification anaglyphs from the surface of four different types of particles that display a variety of unique phenomena associated with lunar regolith. One particular property of lunar regolith is that it sticks to everything including itself. This is due to static buildup from being exposed to the charged particles of the solar wind. Figure 6a shows a glassy region of an agglutinate that is covered with smaller fragments. These fragments can be removed by washing. By contrast, the tiny fragments on the surface of the agglutinate particle shown in Figure 6b have been stuck together by melt flow glass. Notice the tiny ovoid with a hole in its side and the larger sphere only partially exposed to the surface. Figure 6c is an anaglyph of the surface of a glassy particle that is covered in iron globules. A large portion of each globule is, in fact, under the outermost surface with only a small amount breaking through to the outside. XEDS analysis indicates that these globules are primarily iron with trace amounts of nickel and sulfur. Globules of similar composition and morphology have been reported previously by several researchers (e.g., Carter, 1971; Carter & McKay, 1972; Housley et al., 1973; Rode et al., 1979) and are thought to have formed from the condensation of meteor material onto the impact glass while it was still molten. It has also been proposed that iron globules have formed as a result of the reduction of iron silicate in the lunar glass by hydrogen (and possibly carbon) implanted the solar wind during the high-temperature pulse from a micrometeorite impact (McKay et al., 1991). Solar wind reduction of the iron silicate is also thought to be responsible for the formation of *nano*phase Fe^0 particle rims found just below the surface of

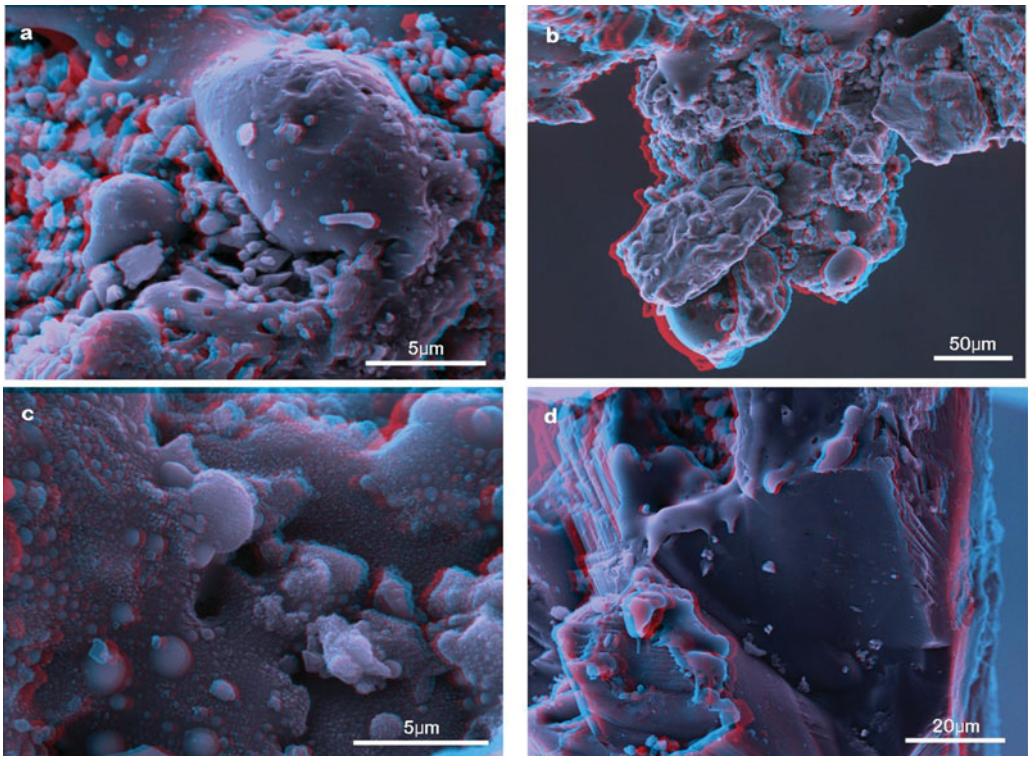

Figure 6. SEM stereo-anaglyphs of (**a**) small mineral and glass fragments electrostatically adhering to the glassy surface of an agglutinate particle (this particle had not been washed with ethanol), (**b**) the surface of an agglutinate particle washed in ethanol showing mineral and glass fragment stuck together by impact glass, (**c**) the surface of a vesicular glass particle containing iron globules, and (**d**) a splash of impact-melt glass on the surface of a faceted mineral particle.

agglutinates and microbreccias (e.g., Keller & McKay, 1997), but these are normally only visible when using a transmission electron microscope. Detailed reviews of how the solar wind interacts with the lunar surface have been published by Lucey et al. (2006) and Pillinger (1979). While the iron globules in the anaglyph shown in Figure 6c look very similar to those reported by McKay et al. (1991) because they contain nickel, it is more likely that they have originated from a micrometeor; without carrying out a more detailed compositional analysis, it is difficult to be certain. Figure 6d shows a splash of impact melt flow glass covering a faceted mineral fragment.

X-Ray Ultramicroscopy

A useful way to highlight the power of this new technique is to compare the corresponding secondary electron and XuM images of the same particle. This allows both the surface morphology and internal structure to be viewed side-by-side. Complementary SEM and XuM micrographs of a 200 μm diameter opaque glassy spherule are shown in Figure 7. The roughened area on top of the spherule (Fig. 7a) suggests that this particle, formed by splashing of molten regolith during a micrometeoroid impact, may not have completely solidified before landing back on the lunar surface. The SEM image also shows several small perforations indicative of internal bubbles, formed by the evolution of trapped gases in the melt, just breaking through the surface. The X-ray image (Fig. 7b) reveals that the particle actually contains a myriad of spherical internal pores, the largest of which has a diameter of 63 μm. Rotation of the sample by 90° (Fig. 7c) shows that this pore has not penetrated the surface. Also clearly visible in Figure 7b,c by absorption

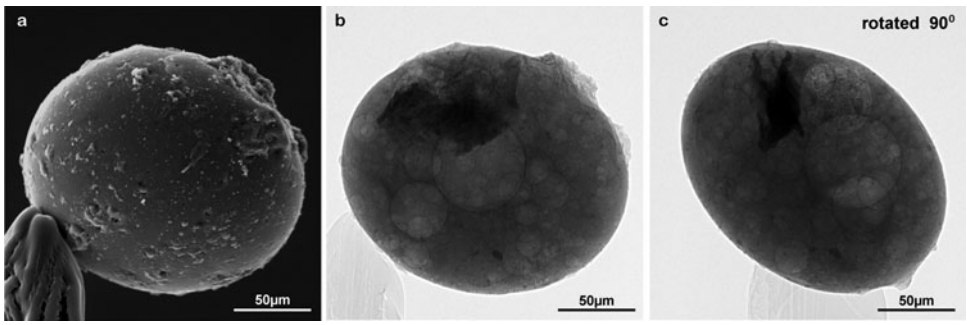

Figure 7. (**a**) A scanning electron and (**b**,**c**) X-ray micrographs of a glass spherule.

contrast is a more dense inclusion. McKay et al. (1970) have previously reported the existence of an ilmenite crystal partially embedded in a similar glassy sphere. An XuM rotational movie of this particle reveals that this inclusion is not a single plate but is made up of a chain of plates arranged at different angles to each other. This movie can be viewed in the supplemental on-line information accompanying this article (see Supplementary Movie 2).

Supplementary Movie 2

Supplementary Movie 2 is an XuM rotational movie of a glassy spherule. Please visit journals.cambridge.org/jid_MAM.

One of the contentious debates concerning glassy lunar particles in the 1970s was whether rod, teardrop, and dumbbell morphologies were formed as a result of (1) the translational breakup of a spray or thin jet of molten regolith (e.g., Chernyak & Nussinov, 1976) or (2) spray droplets gaining rotational momentum and subsequently undergo centrifugation causing their breakup (e.g., Pugh, 1972; Bastin & Volborth, 1974; Bastin, 1980). There is experimental evidence in the literature to support both mechanisms. For example, in an interferometric study of lunar glassy particles, Tolansky (1970) found one long red-brown glass "cylinder" that gave a fringe pattern indicating the onset of it breaking up into three droplets. In a study of Apollo 11 fines, Mueller (1971) observed that the denser phases within a dumbbell particle where located toward its extremities as a result of centrifugation.

Figure 8 shows the XuM images of rod-, teardrop-, and dumbbell-shaped glass particles. All of these particles contain pores, which on closer examination are not quite spherical. There has clearly been some movement in the viscous melt after the bubbles have formed. In the rod-shaped particle, the pores and inclusions appear to be randomly distributed throughout the particle suggesting they may have formed by the translational breakup of a thin jet or spray of molten regolith. Rather than possessing any inclusions, the teardrop has tiny dense particles embedded in its surface. XEDS spot analysis reveals that these consist primarily of iron. In the dumbbell-shaped particle, however, the pores do appear to have migrated toward the center of the dumbbell and the darker inclusions are located at its extremities. This is a clear indication that centrifugation has taken place.

Heiken and Lofgren (1971) found glass spheres similar to those shown in Figure 8 from an eruption of low viscosity ballistic magmas from the 1959 eruption of Kilauea Iki, Hawaii, and also by a TNT-induced surface explosion of alluvium. Both the volcanic and explosion process produced spheres that had analogs in the lunar materials. The volcanic spheres ranged in diameter from 2 μm to several millimeters, but all had smooth surfaces. The explosion-produced spheres are of similar size, but their surfaces are covered with smaller spheres and angular particles. Some eruption-produced spheres contained a large central pore that comprised 80% of the particle volume while others contained several smaller pores.

The reason why these pores are so clearly visible in the X-ray micrographs is because phase contrast is one of the primary contrast mechanisms. Closer inspection of Figures 8 and 9 reveals the presence of a dark and bright Fresnel ring highlighting the edge of every pore. There is also a bright exterior Fresnel fringe surrounding the whole of the particle.

Phase contrast is also very useful for highlighting cracks. Figure 9 shows SEM and XuM micrographs of a solid glass ellipsoid that has experienced two impact events. The larger impact crater exhibits all the classic shockwave-induced features indicative of ballistic impact. Several different types of impact craters on Apollo 11 spherules were reported by several researchers (e.g., Carter & MacGregor, 1970*a*; McKay et al., 1970). Similar impact craters have been found on glassy spherules found in regolith brought back during Luna missions (Hartung et al., 1972; Rode et al., 1979). Carter and MacGregor (1970*a*) attributed these craters to the spherule being pelted by impact-generated particles traveling at velocities up to and including hypervelocity—defined as the velocity required to produce molten glass from solid silicate material on impact. McKay et al. (1970) and Hartung et al. (1972), however, concluded that the craters were formed directly from a micrometeoroid impact. The particle shown in Figure 9 has a high iron content, which degrades the quality of the X-ray image. By carefully altering the contrast of the XuM micrograph, however, the subsurface cracking pattern associated with the smaller impact crater on the top of the particle can still be seen.

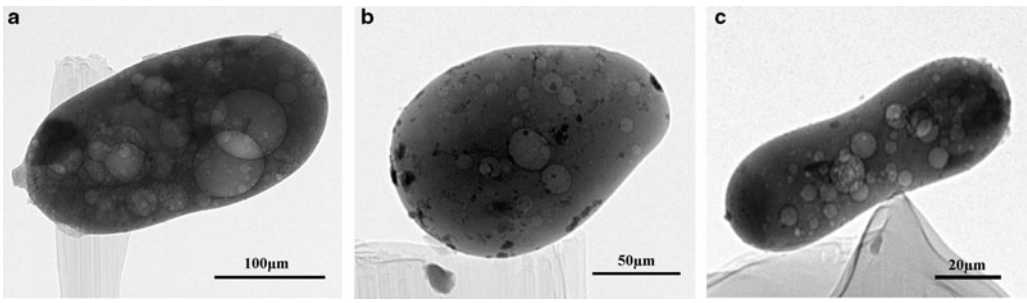

Figure 8. X-ray micrographs of (**a**) a rod-, (**b**) a teardrop-, and (**c**) a dumbbell-shaped particle.

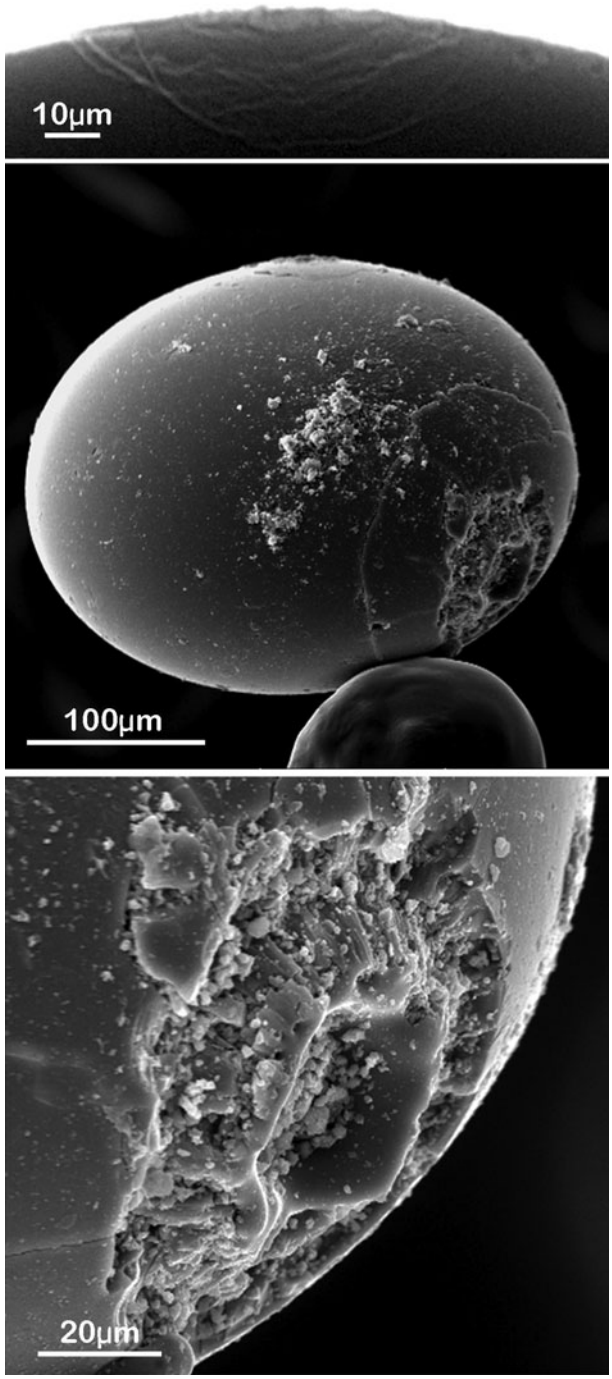

Figure 9. X-ray and scanning electron micrographs of a solid glass spherule showing signs of ballistic impact.

While phase contrast highlights the pores and cracks within a particle, absorption contrast can indicate the presence of more highly absorbing components such as those containing iron and titanium. Dense globules can be seen in the X-ray micrograph of the broken solid sphere shown in Figure 10a. The vast majority of these are located its surface, as confirmed by the SEM image in Figure 10b. The larger globules have reached a diameter close to 8 μm, and there are also several dimples present in the surface where the

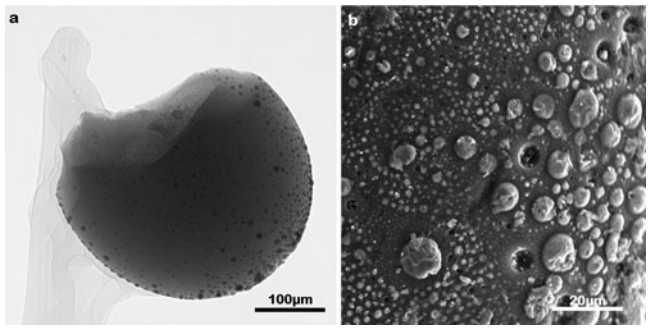

Figure 10. (**a**) An X-ray micrograph of a broken glass sphere containing iron globules together with (**b**) a scanning electron micrograph of its surface.

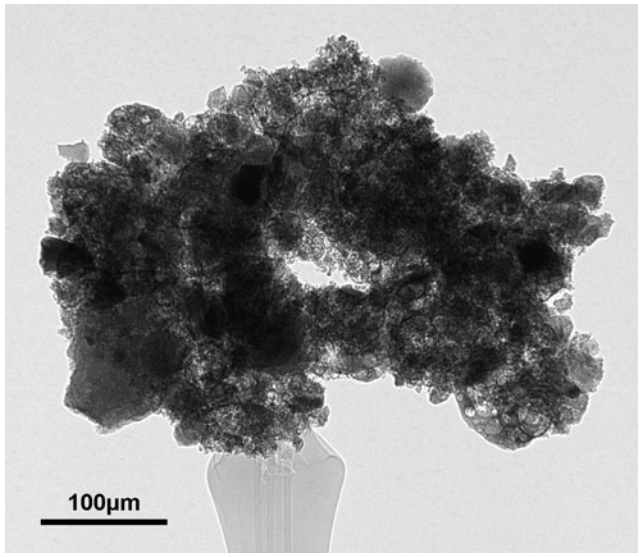

Figure 11. An XuM image of a ring agglutinate.

globules have fallen out. XEDS analysis indicates that while these globules are comprised primarily of iron, they do contain trace amounts of sulfur and nickel, which suggests that at some point the sphere has traveled through an impact-generated cloud of molten iron/nickel and iron sulfide droplets before landing on the lunar surface. There have been several detailed studies of iron/nickel and iron sulfide globules present on the surfaces of lunar regolith particles (e.g., Goldstein et al., 1970; Carter & McKay, 1972), and they have even been seen using a light microscope in a pale blue glassy sphere by Mueller and Hinsch (1970).

The most complicated of all the lunar regolith particles are the agglutinates. Their concentration in a sample of lunar regolith is an indication of the length of time the sample has been exposed to the harsh environment of the lunar surface (McKay et al., 1991). In the case of the Apollo 11 regolith, this is thought to be 3.8 billion years (McKay et al., 1991). An X-ray micrograph of the ring agglutinate shown in Figure 5b is presented in Figure 11. Pores in the glassy matrix are clearly visible, as are the myriad of tiny mineral fragments. The darker block fragments were identi-

fied as ilmenite using XEDS spot analysis. In the past, the size, shape, and spatial distribution of individual fragments contained within agglutinates has been gleaned from analysis of backscattered electron images of polished thin sections (e.g., Heiken & Vaniman, 1990). However, this only provides information from a 2D slice through the particle. Now, for the first time, such information from the entire particle can be gleaned from a rotational XuM movie, which can also be viewed in the supplemental on-line information accompanying this article (see Supplementary Movie 3).

Supplementary Movie 3

Supplementary Movie 3 is an XuM rotational movie of a ring agglutinate. Please visit journals.cambridge.org/jid_MAM.

There are, however, many regolith particles that do not contain pores or vesicular glass. Figure 12 shows the SEM/XuM micrographs of an opaque white anorthositic particle similar to those shown in Figure 2c. The fine grained layered morphology seen in the SEM image is also evident in the X-ray micrograph by the geometrically shaped regions of varying absorption contrast, which do not correspond to thickness variations across the particle. XEDS analysis shows that there is a large variation in chemical composition throughout the particle, the major components being plagioclase and pyroxene. The relative atomic concentration of calcium and iron in the pyroxene components was also found to vary considerably. The darker regions in the X-ray micrograph correspond to those components containing a high atomic concentration of iron. There were also regions containing a relatively high atomic fraction of calcium. Closer examination of both micrographs reveals that this particle is riddled with microcracks.

Ilmenite, $FeTiO_3$, is the most abundant oxide mineral in lunar rocks forming as much a 10% of the Apollo 11 lunar soil. It commonly occurs as bladed crystals up to a few millimeters long and is often closely associated with pyroxene (McKay et al., 1991). In this study, however, ilmenite grains of many different shapes and sizes were detected adjacent to both pyroxene and plagioclase. An example of a particle containing bladed ilmenite grain is shown in Figure 13a,b. The XEDS spectra presented were taken from different regions of the particle. Chemical signatures of calcic plagioclase, pyroxene, and ilmenite were detected. The difference in absorption contrast between the constituent minerals is clearly evident in the X-ray micrograph shown in Figure 13b. Similar XED spectra were also obtained from the particle shown in Figure 13c,d. This particle, however, contains a number of randomly oriented ilmenite plates. The aspect ratio and relative orientation of the ilmenite plates can be easily observed in the XuM rotational movie presented in the supplemental on-line information accompanying this article (see Supplementary Movie 4).

Supplementary Movie 4

Supplementary Movie 4 is an XuM rotational movie of a lunar regolith particle containing plates of ilmenite. Please visit journals.cambridge.org/jid_MAM.

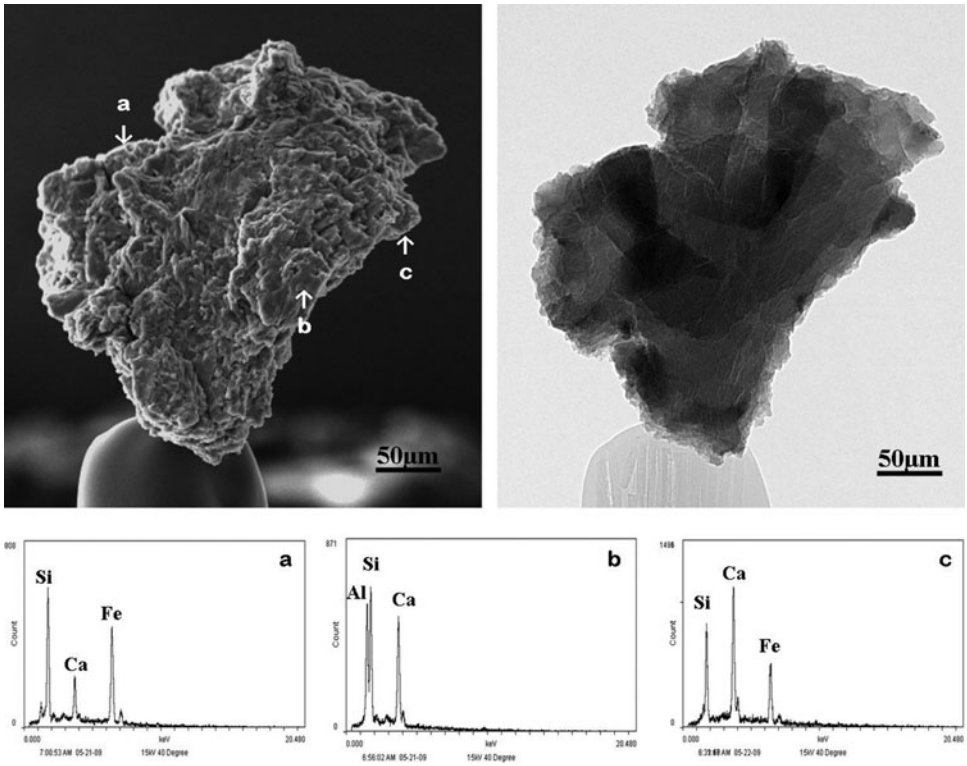

Figure 12. A secondary electron and X-ray micrograph of an opaque white anorthosite particle together with XED spectra taken from highlighted regions of the particle.

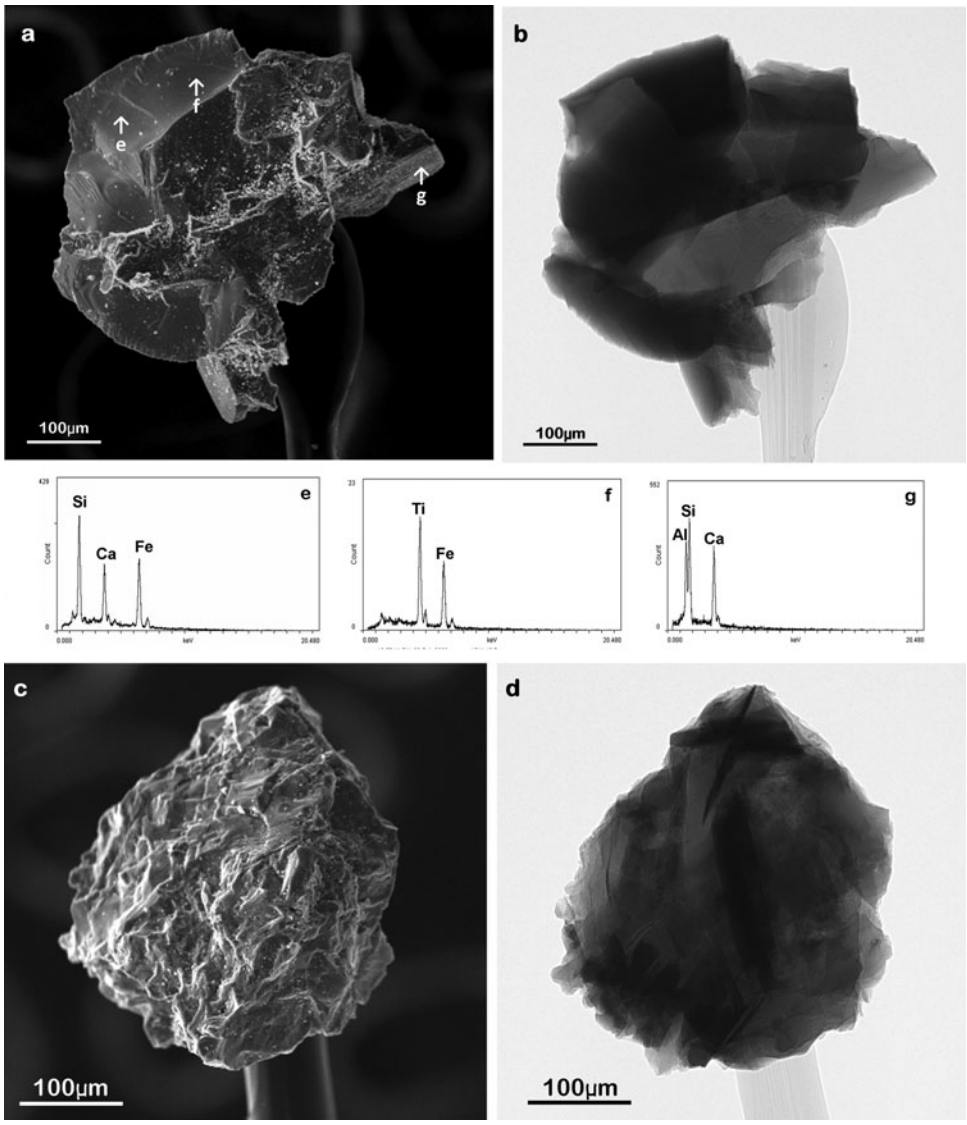

Figure 13. Secondary electron and X-ray micrographs of two particles containing ilmenite. The XEDS spectra have been collected from the highlighted region of the particle shown in panel **a**.

XEDS analysis reveals that the fine-grained particle shown in Figure 14 has components with pyroxene, plagioclase, and ilmenite composition. Even from the SEM images of the surface, it is clear that this particle has many different components including plates and needle-shaped crystals (see Fig. 14d,e). There is even a glassy spherule embedded in the surface. There is also clear evidence that the surface has been splashed with molten regolith from a nearby impact event (see Fig. 14f). In the X-ray micrograph shown in Figure 14b, a number of "dark streaks" are visible. This suggests that the ilmenite exists as stacked sheets rather than the single well-defined plates seen in the previous particle. These are no longer visible in the micrograph taken after the sample has been rotated through 90° (Fig. 14c). There is, however, a new set of "dark stripes" present in this latter micrograph, which corresponds to another set of plates that are oriented perpendicular to the others. It would have been ideal to construct a rotational movie for this particle. However, as with the glassy sphere, shown in Figure 10, this particle's high iron concentration impairs our ability to collect a high-quality image in a reasonable length of time. It took 30 minutes to obtain the single image shown in Figure 14c, which means that the time required to collect enough images to construct a rotational movie is just too prohibitive.

On seeing images of lunar regolith particles for the first time, people often ask, "Is that what it really looks like?" The answer should be, "It depends on what you are using to look at it." Figure 15 shows a complementary set of optical, scanning electron, and X-ray images of the same ring agglutinate. As well as the glassy nature of this particle, the optical image, as one might expect, reveals the variation in color of its different components, from black through brown, orange, and yellow to almost transparent. This image was collected using both oblique transmitted and reflected light. The scanning electron micrograph, on the other hand, shows the surface structure of the particle in greater detail, but the color and the transparent nature of the particle are lost. Notice how the tiny glass sphere on the right-hand side of the particle is much more visible in this micrograph. The XuM image really complements both the optical and the scanning electron data. Regions containing more X-ray ab-

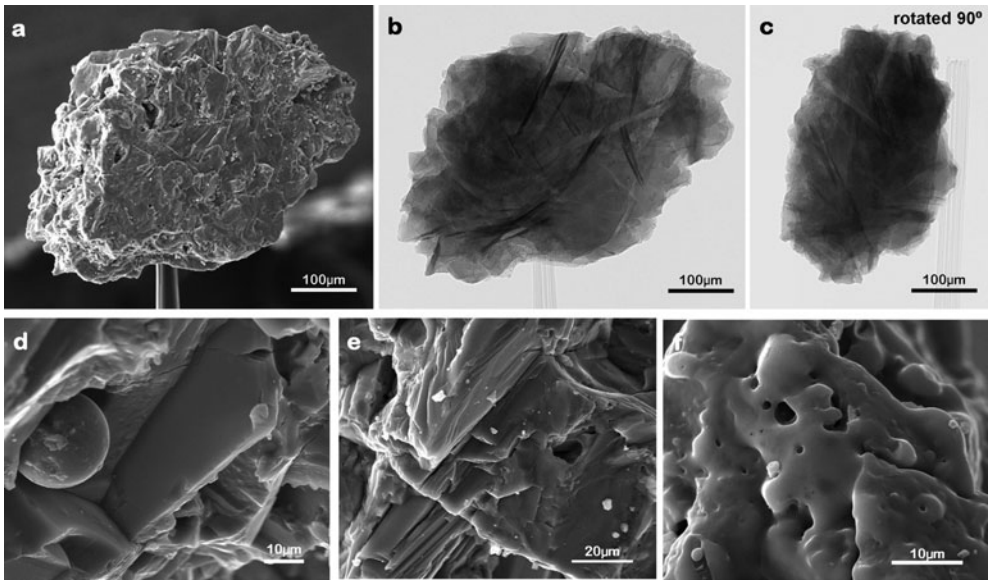

Figure 14. Complementary (**a**) SEM and (**b**) XuM images of a particle containing plagioclase, pyroxene, and ilmenite components; (**c**) XuM image of the particle after 90° rotation; (**d**, **e**, **f**) higher magnification SE micrographs collected from three different surface regions.

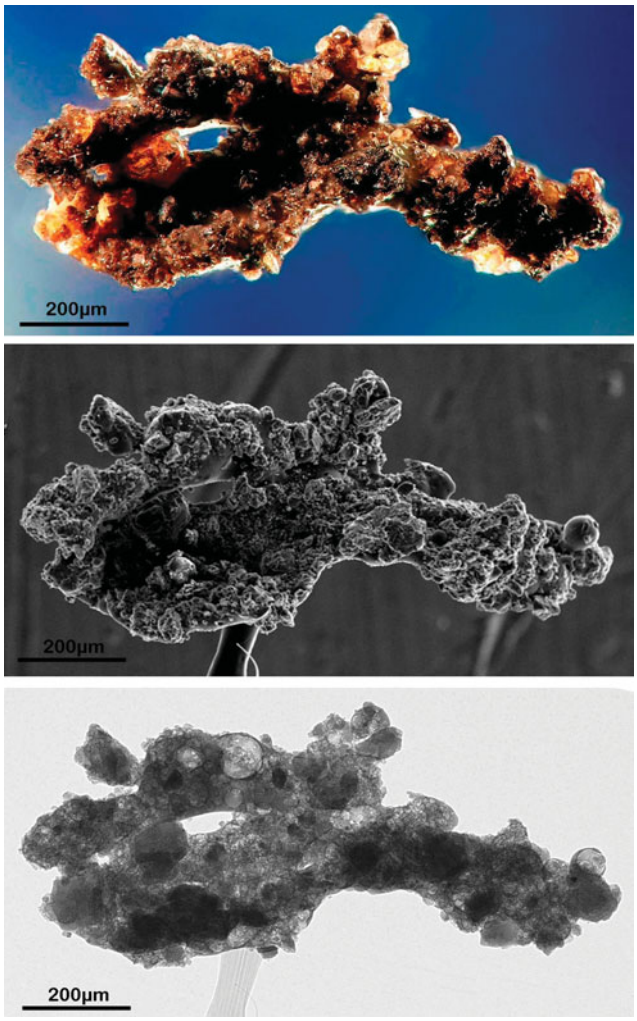

Figure 15. Optical, scanning electron, and X-ray micrographs of a ring agglutinate.

sorbing mineral fragments are clearly visible by absorption contrast, while vesicular glass stands out through phase contrast. It can now be concluded that the glassy sphere so visible in the SEM micrograph was almost certainly formed by an expanding bubble in the glassy melt.

Summary

Combining innovative lighting techniques with state-of-the-art processing of a through focal series of images has allowed us to obtain a collection of optical micrographs showing details that previously could not be accessed via other techniques. In fact, we believe that these are among the best optical images of lunar regolith particles published to date. The ability to collect optical stereo-pairs and being able to view samples in 3D give a dramatically better understanding of their structure. The collection of SEM stereo-pairs is also much under-used and under-rated. In this study, they have proved invaluable in identifying and portraying the nature of the vast array of surface structures. Being able to compare the scanning electron and X-ray images has offered a never-before-seen view of both the surface and internal structure of lunar particles. X-ray ultramicroscopy has provided size, shape, and spatial distribution information on the pores, cracks, and inclusions present in many of these tiny particles. The fact is that the whole 2D projection image of the internal structure is in focus and the ability to collect a rotational series of images offers a much more intuitive, 3D picture. The glass in many agglutinates and spheroids was found to be much more vesicular than expected. XuM does not negate the need to carry out petrographic analysis as it cannot be used to identify specific mineral constituents. It may prove, however, to be an invaluable prescreening tool to pinpoint a particular feature of interest in a particle. Being able to collect optical, scan-

ning electron and X-ray micrographs from the same particle may prove very useful in providing evidence to support or refute existing models on the evolution of lunar regolith.

Acknowledgments

We would like to thank Gene Lucadamo for his help in obtaining the lunar regolith samples from the National Aeronautics and Space Administration (NASA). We are also grateful Julie Sheffield-Parker (XRT), Bill Mushock, Dave Ackland, Bill Hefner, and Arlan Benscoter for their invaluable technical help and expertise. The lunar regolith samples were kindly loaned to Lehigh by the Johnson Space Research Center, NASA under the CAPTEM program. This work was partly funded by a Lehigh/NASA Nanotechnology Agreement.

References

Bastin, J.A. (1980). Rotating lunar globules. *Nature* **283**, 108.

Bastin, J.A. & Volborth, A. (1974). The ellipsoidal and dumbell-shaped inclusions within particulate globules. *Icarus* **21**, 112–120.

Brownlow, L., Mayo, S., Miller, P. & Sheffield-Parker, J. (2006). Towards 50-nanometer resolution with an SEM-hosted X-ray microscope. *Microsc Anal* **12**(3), 13–15.

Burlingame, A.L., Calvin, M., Han, J., Henderson, W., Reed, W. & Simonett, B.R. (1970). Organic compounds in lunar samples: Pyrolysis products, hydrocarbons and amino acids. *Science* **167**, 751–753.

Carter, J.L. (1971). Chemistry and surface morphology of fragments from Apollo 12 soil. *Proc Second Lunar Sci Conf* **1**, 873–892.

Carter, J.L. & MacGregor, I.D. (1970*a*). Minerology, petrology and surface features of lunar samples 10062,35, 10067,9, 10069,30 and 10085,16. *Science* **167**, 661–663.

Carter, J.L. & MacGregor, I.D. (1970*b*). Minerology, petrology and surface features of Apollo 11 samples. *Proc Apollo 11 Lunar Sci Conf* **1**, 247–265.

Carter, J.L. & McKay, D.S. (1972). Metallic mounds produced by reduction of material of a simulated lunar composition and implications on the origin of metallic mounds on lunar glasses. *Proc Third Lunar Sci Conf (Suppl 3: Geochim Cosmochim Acta)* **1**, 953–970.

Chao, C.T., Boreman, J.A., Minkin, J.A., James, O.B. & Desborough, G.A. (1970). Lunar glasses of impact origin: Physical and chemical characteristics and geological implications. *J Geophys Res* **75**(35), 7445–7479.

Chernyak, Yu.B. & Nussinov, M.D. (1976). On the mechanisms of lunar regolith glass formation. *Nature* **261**, 664–669.

Cloud, P., Margolis, S.V., Moorman, M., Barker, J.M., Licari, G.R., Krinsley, D. & Barnes, V.E. (1970). Micromorphology and surface characteristics of lunar dust and breccia. *Science* **167**, 776–777.

Duke, M.B., Woo, C.C., Sellers, G.A., Bird, M.L. & Finkelman, R.B. (1970). Genesis of soil at the tranquility base. *Proc Apollo 11 Lunar Sci Conf (Suppl 1: Geochim Cosmochim Acta)* **1**, 347–361.

Ebel, D.S., Fogel, R.A. & Rivers, M.L. (2005). Tomographic location of potential melt-bearing phenocysts in lunar glass spherules. *Proc 36th Lunar and Planetary Sci Conf*, League City, Texas, March 14–18, 2005, pp. 1505–1506.

Fox, S.W., Harada, K., Hare, P.E., Hinsch, G. & Mueller, G. (1970). Bio-organic compounds and glassy microparticles in lunar fines and other materials. *Science* **167**, 767–770.

Fulchignoni, M., Funiciello, R., Taddeucci, A. & Trigila, R. (1971). Glassy spheroids in lunar fines from Apollo 12 samples 12070,37; 12001,73; and 12057,60. *Proc Second Lunar Sci Conf (Suppl 2: Geochim Cosmochim Acta)* **1**, 937–948.

Goldstein, J.L., Henderson, E.P. & Yakowitz, H. (1970). Investigation of lunar metal particles. *Proc Apollo 11 Lunar Sci Conf* **1**, 499–512.

Greenberg, G. (2008). *A Grain of Sand: Nature's Secret Wonder*. Minneapolis, MN: Voyageur Press.

Greenberg, G. & Boyde, A. (1993). Novel method for stereo imaging in light microscopy at high magnifications. *NeuroImage* **1**(2), 121–128.

Greenberg, G. & Boyde, A. (1997). Convenient and controllable direct-view 3D imaging in conventional light microscopes: Approaches via illumination and inspection. *Proc Royal Microsc Soc* **32**, 87–100.

Hartung, J.B., Horz, F., McKay, D.S. & Baiamonte, F.L. (1972). Surface features on glass spherules from the Luna 16 sample. *The Moon* **5**, 436–446.

Heiken, G. & Lofgren, G. (1971). Terrestrial glass spheres. *Geol Soc Am Bull* **82**, 1045–1050.

Heiken, G.H., McKay, D.S. & Brown, R.W. (1974). Lunar deposits of possible pyroclastic origin. *Geochim Cosmochim Acta* **38**, 1703–1704.

Heiken, G.H. & Vaniman, D.T. (1990). Characterization of lunar ilmenite resources. *Proc 20th Lunar and Planetary Sci Conf*, Houston, Texas, March 1989, pp. 239–247.

Housley, R.M., Grant, R.W. & Paton, N.E. (1973). Origin and characteristics of excess Fe metal in lunar glass welded aggregates. *Proc Fourth Lunar Sci Conf (Suppl 4: Geochim Cosmochim Acta)* **3**, 2737–2749.

Keller, L.P. & McKay, D.S. (1997). The nature and origin of rims on lunar soil grains. *Geochim Cosmochim Acta* **64**(11), 2331–2341.

Lindsey, J. (1976). *Developments in Solar System and Space Science, 3 Lunar Stratigraphy and Sedimentology*. Kopa, Z. & Cameron, A.G.W. (Eds.). New York: Elsevier Scientific Publishing Company.

Lindsay, J.F. & Srnka, L.J. (1975). Galactic dust lanes and lunar soil. *Nature* **257**, 776–778.

Lucey, P., Korotev, R.L., Gillis, J.J., Taylor, L.A., Lawrence, D., Campbell, B.A., Elphic, R., Feldman, B., Hood, L.L., Hunter, D., Mendilli, M., Noble, S., Papike, J.J., Reedy, R.C., Lawson, S., Prettyman, T., Gasnault, O. & Maurice, S. (2006). Understanding the lunar surface and space-moon interactions, new views of the moon. *Rev Mineral Geochem* **60**, 83–219.

Lui, Y., Park, J., Schnare, D., Hill, E. & Taylor, L.A. (2008). Characterization of lunar dust for toxicological studies II: Texture and shape. *J Aerosp Eng* **21**(10), 272–279.

McKay, D.S., Greenwood, W.R. & Morrison, D.A. (1970). Origin of small lunar particles and breccia from the Apollo 11 site. *Proc Apollo 11 Lunar Sci Conf* **1**, 673–694.

McKay, D.S., Heiken, G., Basu, A., Blanford, G., Simon, S., Reedy, R., French, B.M. & Papike, J. (1991). The lunar regolith. *Lunar Sourcebook: A User's Guide to the Moon*, Chap. 7, pp. 285–356 New York: Cambridge University Press.

Morris, R.V., Score, R., Dardano, C. & Heiken, G. (1983). *Apollo 11 Samples Data Sheet in the Handbook of Lunar Soils*, JSC 19069, Washington, DC: NASA.

Mueller, G. (1971). Morphology and petrostatistics of regular particles in Apollo 11 and Apollo 12 fines. *Proc Second Lunar Sci Conf* **3**, 2041–2047.

Mueller, G. & Hinsch, G.W. (1970). Glassy particles in lunar fines. *Nature* **228**, 254–258.

Nagy, B., Drew, C.M., Hamilton, P.B., Modzeleski, V.E., Murphy, M.E., Scott, W.M., Urey, H.C. & Young, M. (1970). Organic compounds in lunar samples: Pyrolysis products, hydrocarbons, amino acids. *Science* **167**, 770–773.

Pawley, J.B. (Eds.) (1995). *Handbook of Biological Confocal Microscopy*. New York: Plenum Press.

Pillinger, C.T. (1979). Solar-wind exposure effects in the lunar soil. *Rep Prog Phys* **42**, 897–967.

Pugh, M.J. (1972). Rotation of lunar dumbell-shaped globules during formation. *Nature* **237**, 158–159.

Ramsamooj, R., Doolin, E., Greenberg, G., Catalano, E. & Hewitt, C.W. (2002). Real-time, high-definition, three-dimensional microscopy of evaluating problematic cervical papanicolaou smears classified as atypical squamous cells of undetermined significance. *Cancer Cytophathol* **96**(3), 181–186.

Robens, E., Bischoff, A., Schreiber, A., Dabrowski, A. & Unger, K.K. (2007). Investigation of the surface properties of lunar regolith: Part 1. *Appl Surf Sci* **253**, 5709–5714.

Rode, O.D., Ivanov, A.V., Nazarov, M.A., Cimbalnikova, A., Jurek, K. & Hejl, V. (1979). *Atlas of Photomicrographs of the Surface of Structures of Lunar Regolith Particles*. Prague: Academia.

Taylor, L.A., Patchen, A., Taylor, D-H.S., Chambers, J.G. & McKay, D.S. (1996). X-ray digital imaging petrography of lunar mare soils: Mode analyses of minerals and glasses. *Icarus* **124**, 500–512.

Tolansky, S. (1970). Interferometric examination of small glassy spherules and related objects in a 5-gram lunar dust sample. *Science* **167**, 742–743.

Wilkins, S.W., Gureyev, T.E., Gao, D., Pogany, A. & Stevenson, A.W. (1996). Phase-contrast imaging using polychromatic hard X-rays. *Nature* **384**, 335–338.